Weak coupling limit of U(1) lattice model in Fourier basis

Afsaneh Kianfar and Amir H. Fatollahi*

Department of Physics, Faculty of Physics and Chemistry, Alzahra University, Tehran 1993891167, Iran

(Received 10 June 2022; revised 9 September 2022; accepted 30 September 2022; published 17 October 2022)

The transfer matrix of the U(1) lattice model is considered in the Fourier basis and in the weak coupling limit. The issues of Gauss law constraint and gauge invariant states are addressed in the Fourier basis. In particular, it is shown that in the strong coupling limit the gauge invariant Fourier states are effectively the finite size closed loop currents. In the weak coupling limit, however, the link currents along periodic or infinite spatial directions find comparable roles as gauge invariant states. The subtleties related to the extreme weak coupling of the transfer matrix in the Fourier basis are discussed. A careful analysis of the zero eigenvalues of the matrix in the quadratic action leads to a safe extraction of the diverging group volume in the limit $g \to 0$. By means of the very basic notions and tools of the lattice model, the spectrum at the weak coupling limit for any dimension and size of lattice is obtained analytically. The spectrum at the weak coupling limit corresponds to the expected one by the continuum model in the large lattice limit.

DOI: 10.1103/PhysRevD.106.074504

I. INTRODUCTION AND OUTLINE

In spite of the incomparable advantages of lattice gauge models for theoretical and practical purposes in the strong coupling regime, a full understanding of the weak coupling limit is still an open issue. In particular, the lattice gauge models are usually transferred to the extreme weak (arbitrary small) coupling regime in an uncontrolled way, leaving shortcomings and unresolved issues, specifically as follows:

(1) Although the distinguished role of the Wilson loops is well appreciated in the strong coupling limit, it is not quite understood which subset of these gauge invariant quantities has the main role in the weak coupling regime.

(2) In going to the extreme weak coupling limit, the exact point at which the diverging contribution of the unfixed gauge degrees comes into the calculation is not well identified. Further, a way of safe and controlled extraction of the diverging contribution, the so-called group volume, is still lacking.

(3) Once the above two issues are fixed, as a matter of necessity, the lattice model has to recover the continuum part of the spectrum expected by the classical model in any dimension.

It is the purpose of the present work to address the above issues for the pure U(1) lattice gauge model in the temporal gauge. In particular, the transfer matrix of the model is studied in the field Fourier basis. The lattice gauge models in Fourier basis have been studied since the early years of these models. The plaquette degrees in Fourier basis, the so-called dual variables [1], are used to present a qualitative description of the phases by the U(1) model in different dimensions [2]. The numerical studies based on the dual formulation show a clear advantage of using integer variables compared to the original continuous ones [3]. The Fourier transform of the links variables also is known as the electric flux basis. The basis is used in a numerical setup of the Hamiltonian formulation of the lattice models [4–6]. Following [7,8], the present application of the Fourier transform is also for gauge link variables appearing in the transfer matrix of the model. The associated Fourier variables again appear to be integer valued, and they are interpreted as quantized currents on the lattice links [7]. In [7,8] it was shown that the transfer matrix in the Fourier basis is block diagonal. In fact, as a consequence of a lattice version of the local current conservation, the current-states differing in the loop-currents circulating inside plaquettes belong to the same block [7]. The members of each block can be constructed by an arbitrary member of the block as the representative [7]. A diagrammatic representation was introduced in [7] for the strong coupling expansion of the transfer-matrix elements in the Fourier basis. With g as the gauge coupling, the parameter of expansion is $1/g^2$, which is small in the strong coupling limit. The expansion of the matrix-element between two current-states of the same block is directly interpreted as the occurrence of all possible virtual link and

*Corresponding author.
fath@alzahra.ac.ir

Published by the American Physical Society under the terms of the Creative Commons Attribution 4.0 International license. Further distribution of this work must maintain attribution to the author(s) and the published article's title, journal citation, and DOI. Funded by SCOAP³.

loop currents that transform the current states to the vacuum (the state with no current). Based on the expansion of the transfer-matrix elements in the Fourier basis, it was shown that the low lying energy levels can be calculated by means of the simple perturbative methods in the strong coupling regime [7].

Based on notions and expressions developed in [7], as far as the transfer matrix of the U(1) gauge model in the Fourier basis is concerned, it is shown that the above-mentioned issues can be addressed as the following:

(1) In the Fourier basis the Wilson loops are represented by the current states with no boundary, which are either current loops belonging to the vacuum block, or states with equal links currents along a periodic or an infinite spatial direction. While in the strong coupling limit the closed currents of the vacuum block have the main contribution to the transfer matrix, in the weak coupling regime the link currents along spatial directions also find comparable roles.

(2) In the extreme weak coupling limit, the zero eigenvalues of the matrix in the quadratic action can be identified as the origin of the diverging contributions to the elements of the transfer matrix in the Fourier basis. The states belonging to the subspace corresponding to the zero eigenvalues are clearly interpreted as pure gauge configurations, on which the matrix in the quadratic action vanishes. The dimension, as well as the diverging volume of the subspace in the weak coupling limit, can be handled in a safe and controlled way.

(3) By means of the very basic notions and tools of the lattice model, the spectrum at weak coupling limit for any dimension and size of lattice is obtained analytically. The spectrum consists of the sum of possible energies by static and standing wave field configurations on the lattice. In the large lattice limit the spectrum at the weak coupling limit corresponds to the expected one by the continuum model.

One of the basic tools used in the formulation of the transfer matrix in the Fourier basis is the plaquette-link matrix $\boldsymbol{M}$ [7,8], by which the elements defined on the lattice can be managed at any coupling. As a consequence, it is seen that the matrix $\boldsymbol{M}$ provides the possibility to keep and work with the fundamental lattice notions even in the extreme weak coupling limit. On the other hand, using this matrix enables to translate the tools in the continuum model, such as spatial derivatives, into the lattice model. These all make it possible to calculate the dimension of the subspace by the mentioned zero eigenvalues and to control the group volume.

The rest of the paper is organized as follows. In Sec. II, a short review of the formulation of the transfer matrix in the Fourier basis, together with a detailed description of emerging notions, are presented. In Sec. III the condition by which the gauge invariant states are identified, the so-called Gauss law constraint, is discussed. Section IV presents the weak coupling limit of the transfer-matrix elements, together with the subtleties related to the diverging group volume and its treatment. In Sec. V it is shown how the continuum part of the spectrum can be recovered in the small coupling limit of the lattice gauge model. Section VI is devoted to concluding remarks. A detailed comparison between the lattice model in the weak coupling limit and the continuum model is presented in Appendix A. The calculation of relevant eigenvalues is presented in Appendix B.

II. REVIEW: CURRENT EXPANSION IN FOURIER BASIS

In this section, the formulation of the transfer matrix in the Fourier basis based on [7,8] is shortly reviewed. In particular, the elements and notions emerged through the Fourier transform, specially in connection with the current interpretation of the Fourier modes, are emphasized. Following [9,10], the temporal gauge $A^0 \equiv 0$ is used in the formulation. The link "l" at site $\boldsymbol{r}$ in spatial direction "i" is represented by $l = (\boldsymbol{r}, i)$. The gauge variables at adjacent times n_t and $n_t + 1$ are introduced to the model as follows:

$$n_t\colon\ \theta^l = agA^{(\boldsymbol{r},i)}, \tag{1}$$

$$n_t + 1\colon\ \theta'^l = agA'^{(\boldsymbol{r},i)} \tag{2}$$

taking values in $[-\pi, \pi]$ [11,12]. Above, "g" and "a" are the gauge coupling and the lattice spacing parameters, respectively. For a spatial lattice with N_{L} number of links and N_{P} number of plaquettes, it is helpful to define the plaquette-link matrix $\boldsymbol{M}$ of dimension $N_{\mathrm{P}} \times N_{\mathrm{L}}$, as following explicitly by its elements

$$M_l^p = \begin{cases} \pm 1, & \text{link } l = (\boldsymbol{r}, \pm i) \text{ belongs to oriented plaquette } p \\ 0, & \text{otherwise} \end{cases}. \tag{3}$$

In Fig. 1 a graphical representation of the definition is given. Setting

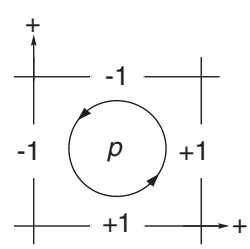

FIG. 1. Graphical representation of definition (3).

$$\gamma = \frac{1}{g^2} \tag{4}$$

the elements of the transfer matrix $\hat{V}$ are defined in terms of the Euclidean action between two adjacent times [7]

$$\langle \boldsymbol{\theta}' | \hat{V} | \boldsymbol{\theta} \rangle = \mathcal{A} \prod_p \exp\left\{ -\frac{\gamma}{2} [2 - \cos(M^p{}_l \theta^l) - \cos(M^p{}_l \theta'^l)] \right\} \times \prod_l \exp\{-\gamma[1 - \cos(\theta^l - \theta'^l)]\}, \tag{5}$$

in which the summations over repeated indices are understood. In the above $\mathcal{A}$ is inserted to fix the normalization [13], an issue we will come back to it in Secs. III and IV. The Fourier basis $|k_l\rangle$ is related to the compact θ basis by

$$\langle \theta'' | k_l \rangle = \frac{\delta^{l''}{}_l}{\sqrt{2\pi}} \exp(\mathrm{i}\, k_l \theta^l), \qquad k_l = 0, \pm 1, \pm 2, \cdots \tag{6}$$

by which the transfer-matrix elements in the Fourier basis can be found

$$\langle \boldsymbol{k}' | \hat{V} | \boldsymbol{k} \rangle = \frac{1}{(2\pi)^{N_\mathrm{L}}} \int_{-\pi}^{\pi} \prod_l \mathrm{d}\theta'_l \mathrm{d}\theta_l e^{-\mathrm{i}\boldsymbol{k}'\cdot\boldsymbol{\theta}'} e^{\mathrm{i}\boldsymbol{k}\cdot\boldsymbol{\theta}} \langle \boldsymbol{\theta}' | \hat{V} | \boldsymbol{\theta} \rangle \tag{7}$$

Accordingly, it is shown that $\hat{V}$ is block diagonal in the Fourier basis [7,8], and all elements of a block can be presented by an arbitrary block's member $\boldsymbol{k}_*$ as the representative, whose coblocks are all constructed as

$$\boldsymbol{k}_{*\boldsymbol{q}} = \boldsymbol{k}_* + \boldsymbol{q} \cdot \boldsymbol{M} \tag{8}$$

in which $\boldsymbol{q}$ is a row vector with N_P integers as components. It will be seen later, as a manifestation of the current conservation, two coblocks can differ at most in the circulating currents inside plaquettes, allowing to have a nonzero matrix element. Consequently, the matrix element between two coblocks represented by $\boldsymbol{k}_*$ is found to be [7]

$$\langle \boldsymbol{k}'_{*\boldsymbol{q}'} | \hat{V} | \boldsymbol{k}_{*\boldsymbol{q}} \rangle = \mathcal{A} e^{-\gamma(N_\mathrm{P}+N_\mathrm{L})} (2\pi)^{N_\mathrm{L}} \times \sum_{\{n_p^0\}} \sum_{\{n_p\}} \prod_p \mathrm{I}_{q_p - n_p}\left(\frac{\gamma}{2}\right) \mathrm{I}_{q'_p - n_p + n_p^0}\left(\frac{\gamma}{2}\right) \times \prod_l \mathrm{I}_{k_* + \sum_p n_p M^p{}_l}(\gamma), \tag{9}$$

in which $\boldsymbol{k}_{*\boldsymbol{q}}$ is given by (8), and

$$\boldsymbol{k}'_{*\boldsymbol{q}'} = \boldsymbol{k}_* + \boldsymbol{q}' \cdot \boldsymbol{M}. \tag{10}$$

In (9), all summations are on integers, and I_rs are modified Bessel functions. Further, in a vector notation, n_p^0s satisfy the following relation (including $\boldsymbol{n}^0 = \boldsymbol{0}$) [7]:

$$\boldsymbol{n}^0 \cdot \boldsymbol{M} = \boldsymbol{0}. \tag{11}$$

Before proceeding to the strong coupling expansion, it is quite insightful to discuss the physical meaning of the objects that emerged in the Fourier basis. First is the Fourier vector $\boldsymbol{k}$ itself, which can be directly understood by its appearance, namely by (7), and its similar expression in the continuum theory, by the coupling of the current J to the gauge field A

$$e^{\mathrm{i}\sum_l k_l \theta^l} = e^{\mathrm{i}\, a\, g \sum_l k_l A^l} \to e^{\mathrm{i}g \int J \cdot A dx}. \tag{12}$$

Above, k_l is interpreted as the number of the current quanta coupled to the gauge field A^l associated to the link "l." Accordingly, the current vector $\boldsymbol{k}$ consists of the link currents k_ls. The integer value of k_l reflects the fact that, thanks to the compact nature of gauge fields in the lattice model, the quantization of charge is satisfied automatically. By the above interpretation of k_ls, the Fourier basis $|\boldsymbol{k}\rangle$ is representing the states of current quanta on the lattice links. Now, by the definition of the transfer-matrix $\hat{V} = \exp(-a\hat{H})$, with $\hat{H}$ as the Hamiltonian, the matrix element $\langle \boldsymbol{k}' | \hat{V} | \boldsymbol{k} \rangle$ is the transition amplitude between the states with $\boldsymbol{k}$ and $\boldsymbol{k}'$ currents during the imaginary time interval "a."

To find the meaning of the integers q_ps, first we need to realize the role of the matrix $\boldsymbol{M}$, defined by its elements in (3). In [7,8], an explicit representation of this matrix for the 2D spatial lattice is presented; see also the Appendices of the present work. Accordingly, by the definition (3) each q_p turns on two $+q_p$s and two $-q_p$s units of currents in four links of plaquette "p," being added to already existing currents of $\boldsymbol{k}_*$ in (8) [7,8]. As an example, let us consider the block represented by the vacuum state $\boldsymbol{k}_* = \boldsymbol{k_0} = \boldsymbol{0}$, and its coblock

$$\boldsymbol{k}_{\boldsymbol{0};\boldsymbol{1}} = \boldsymbol{k_0} + \boldsymbol{q_1} \cdot \boldsymbol{M}, \tag{13}$$

with N_P-component vector $\boldsymbol{q_1} = (1, 0, \ldots, 0)$. Equation (13) is pictorially presented in Fig. 2, showing that the resulting vector current has only four links with a nonzero current, namely two $+1$s and two -1s, making a circulating unit current in the first plaquette. As seen, q_p is determining the

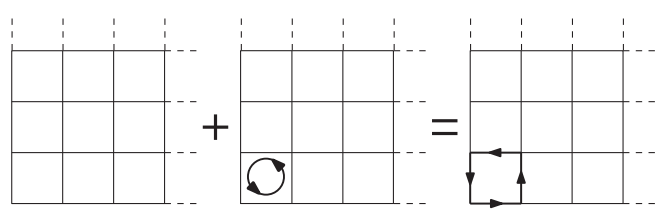

FIG. 2. The graphical representation of (13) to construct $\boldsymbol{k}_{\boldsymbol{0};\boldsymbol{1}}$ as a coblock of $\boldsymbol{k_0} = \boldsymbol{0}$.

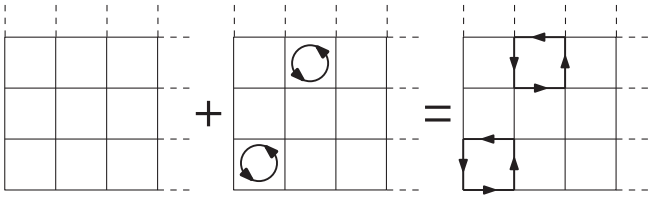

FIG. 3. Construction of a coblock of $\boldsymbol{k_0}$ with two nonadjacent plaquette currents.

number of current quanta circulating in the plaquette "p." It is befitted to call the q_p numbers as plaquette currents or loop currents. As another example from the vacuum block, consider the state constructed by all q_ps zero, except two of nonadjacent plaquettes, as depicted in Fig. 3. By above interpretation of q_ps, the transfer-matrix elements are nonzero only between the current states that differ in circulating currents inside plaquettes, as a consequence of the current conservation [7].

Let us go beyond the vacuum block by considering the state represented by the N_{L}-component vector current $\boldsymbol{k_1} = (1, 0, \ldots, 0)$, which has one unit of current on the first link of the lattice, with all other link currents zero. It is easy to see that there is no set of loop currents $\boldsymbol{q} \cdot \boldsymbol{M}$ that could yield this vector from any member of the vacuum block. Two coblocks of this state are presented in Figs. 4 and 5 [7].

One of the most special blocks is the one represented by the vacuum state $\boldsymbol{k_0} = \boldsymbol{0}$. In [8] it is shown that, provided that the ground state is unique, it belongs to $\boldsymbol{k_0}$'s block. The reason simply backs to the fact that in the extreme large coupling limit $g \to \infty$ ($\gamma \to 0$), as all elements except V_{00} are approaching zero, using the fact the energy and $\hat{V}$ eigenvalues are related as

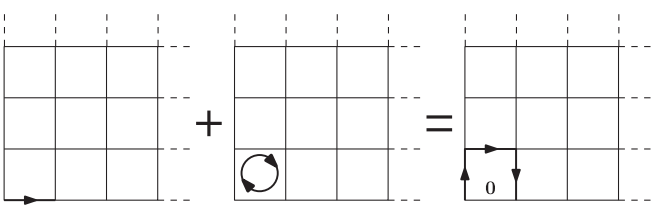

FIG. 4. $\boldsymbol{k_{1;-1}} = \boldsymbol{k_1} - \boldsymbol{q_1} \cdot \boldsymbol{M}$ as a coblock of $\boldsymbol{k_1}$ with three links having unit current.

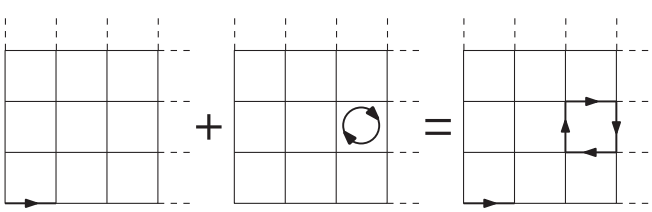

FIG. 5. A coblock of $\boldsymbol{k_1}$ with five links having unit current.

$$E_i = -\frac{1}{a} \ln v_i \tag{14}$$

the ground state belongs to the vacuum block. By uniqueness of the ground state, upon lowering the coupling, no crossing between ground state by other states occurs, leaving the ground states in the vacuum block at any coupling [8].

The presented interpretation of $\boldsymbol{k}$ and $\boldsymbol{q}$ as link and loop currents leads to a diagrammatic strong coupling expansion of the transfer matrix in the Fourier basis [7]. Specifically, it is shown that the elements of the transfer matrix between two states of a block can be represented as a sum over occurrences of the virtual loop and link currents that transform both states to the vacuum [7]. In other words, the transition between two states, represented by the element $\langle \boldsymbol{k}' | \hat{V} | \boldsymbol{k} \rangle$, occurs as if the vacuum state is being passed as an intermediate state [7]. The transformation to the vacuum via occurrences of the virtual currents is to be considered even for states that do not belong to the vacuum block. This is because the coblocks of a state are determined by adding loop currents via $\boldsymbol{q} \cdot \boldsymbol{M}$ as (8), but the mentioned transform to the vacuum is due to both link and loop currents, the former via "$\cos(\theta - \theta')$" term that is irrelevant for making coblocks. It is due to these link currents that transformation of any state, including those from other blocks, into the vacuum is made possible [7]. The distinguished role of the vacuum state simply comes back to the fact that the Fourier integrals over $\boldsymbol{\theta}$ and $\boldsymbol{\theta}'$ related to both states are to be satisfied separately, namely $\boldsymbol{k} \to \boldsymbol{0}$ and $\boldsymbol{k}' \to \boldsymbol{0}$ [7].

To present the diagrammatic expansion, let us use the normalized transfer matrix as

$$\hat{V} = \mathcal{A} e^{-\gamma(N_{\mathrm{L}} + N_{\mathrm{P}})} (2\pi)^{N_{\mathrm{L}}} \underline{\hat{V}}, \tag{15}$$

by which $\langle \boldsymbol{0} | \underline{\hat{V}} | \boldsymbol{0} \rangle = 1 + \mathrm{O}(\gamma^2)$. For two given states of $|\boldsymbol{k}\rangle$ and $|\boldsymbol{k}'\rangle$ in a block, consider the case that they transform to the vacuum by m and m' numbers of the virtual loop-currents, respectively, accompanied by ℓ numbers of the virtual link currents for both states. Now, the numerical factor associated with the matrix element of transition through the mentioned transform is [7]

$$[\langle \boldsymbol{k}' | \underline{\hat{V}} | \boldsymbol{k} \rangle]_{m,m',\ell} = \mathcal{K}_{m,m',\ell} \frac{1}{2^{2m+2m'+\ell}} \frac{1}{m! m' ! \ell !} \gamma^{m+m'+\ell}, \tag{16}$$

in which $\mathcal{K}_{m,m',\ell}$ is the combinatorial factor representing the number of ways that loop and link currents can be combined, regarding the initial and final transformations to the vacuum. As mentioned, the above matrix elements can be represented by a set of graphs in which a proper combination of virtual loop and link currents would make the required pass through the vacuum. The ways that the

initial and final states transform to the vacuum, accompanied by the associated numerical and combinatorial factors of each transition, simply fix the terms in the strong coupling expansion [7]. In this respect, these graphical representations can serve as the Feynman diagrams in the perturbative quantum field theory. The elements being used in graphs are simply the currents, loop or link ones, being characterized by their real or virtual natures. Accordingly, the initial and final states, being determined only by the link currents, are interpreted as real and presented by a combination of solid lines as

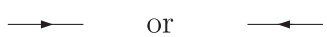

(17)

and their rotated versions. Instead, the loop and link currents occurred during the transforms are interpreted as virtual, being drawn in dashed form as below for the loop currents

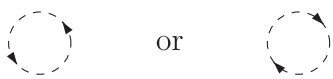

(18)

and the following for link currents

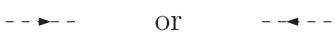

(19)

To emphasize the pass through the vacuum, we use the notation $\boldsymbol{k}' \xrightarrow{0} \boldsymbol{k}$ for the matrix element $\langle \boldsymbol{k}'|\underline{\hat{V}}|\boldsymbol{k}\rangle$ [7]. As examples of the diagrammatic representation of the terms in the strong coupling expansion, the diagrams contributing to the vacuum to vacuum transition at order γ^2 are

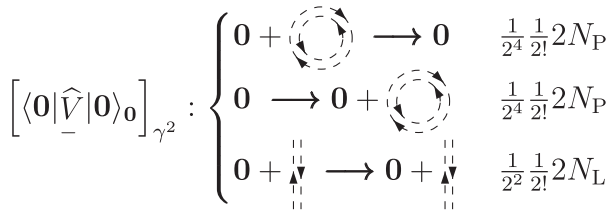

(20)

in which, as before, N_{P} and N_{L} are number of plaquettes and link in the lattice, respectively. At order γ^4, denoting

$$C_n^m = \binom{n}{m} = \frac{n!}{m!(n-m)!}, \tag{21}$$

we have the following

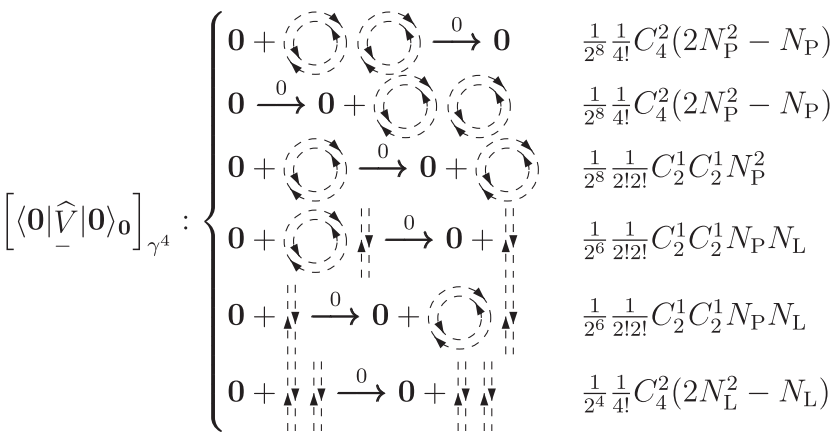

(22)

All together we have [7]

$$\langle \mathbf{0}|\underline{\hat{V}}|\mathbf{0}\rangle_{\mathbf{0}} = 1 + \left(\frac{N_{\mathrm{P}}}{8} + \frac{N_{\mathrm{L}}}{4}\right)\gamma^2 + \left(-\frac{N_{\mathrm{L}}}{64} + \frac{N_{\mathrm{L}}^2}{32} - \frac{N_{\mathrm{P}}}{512} + \frac{N_{\mathrm{P}}N_{\mathrm{L}}}{32} + \frac{N_{\mathrm{P}}^2}{128}\right)\gamma^4 + \mathrm{O}(\gamma^6). \tag{23}$$

Similarly, denoting $\boldsymbol{k}_{\mathbf{0};\mathbf{1}}$ as $|\mathbf{1}\rangle$, for the transition $\mathbf{1} \xrightarrow{0} \mathbf{1}$ we have

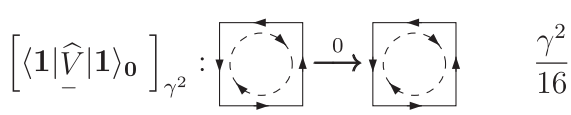

(24)

and

$$\left[\langle \mathbf{1}|\underline{\widehat{V}}|\mathbf{1}\rangle_{\mathbf{0}}\right]_{\gamma^4}:$$

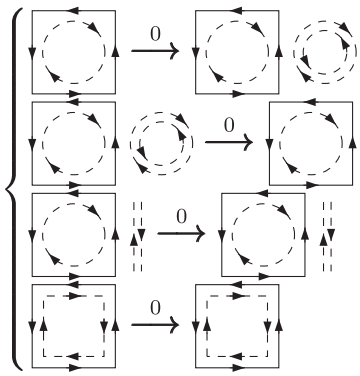

$$\frac{1}{2^8}\frac{1}{3!}C_3^1(2N_{\mathrm{P}}-1)$$

$$\frac{1}{2^8}\frac{1}{3!}C_3^1(2N_{\mathrm{P}}-1)$$

$$\frac{1}{2^6}\frac{1}{2!}C_2^1 N_{\mathrm{L}}$$

$$\frac{1}{2^4}\frac{1}{4!}C_4^2\, 4 \tag{25}$$

leading to

$$\langle \mathbf{1}|\underline{\hat{V}}|\mathbf{1}\rangle_{\mathbf{0}} = \frac{\gamma^2}{16} + \left(\frac{15}{256} + \frac{N_{\mathrm{L}}}{64} + \frac{N_{\mathrm{P}}}{128}\right)\gamma^4 + \cdots. \tag{26}$$

As final sample of the strong coupling expansion we find for the $\mathbf{1} \xrightarrow{0} \mathbf{0}$ transition

$$\langle \mathbf{1}|\underline{\hat{V}}|\mathbf{0}\rangle_{\mathbf{0}} = \frac{\gamma}{4} + \left(\frac{-1}{128} + \frac{N_{\mathrm{P}}}{32} + \frac{N_{\mathrm{L}}}{16}\right)\gamma^3 + \left(\frac{49}{3072} - \frac{3N_{\mathrm{L}}}{512} + \frac{N_{\mathrm{L}}^2}{128} - \frac{3N_{\mathrm{P}}}{2048} + \frac{N_{\mathrm{L}}N_{\mathrm{P}}}{128} + \frac{N_{\mathrm{P}}^2}{512}\right)\gamma^5 + \cdots. \tag{27}$$

Many other examples of the diagrammatic expansion in the strong coupling limit are presented in [7]. For a general matrix element, it can be shown that two subsequent orders of γ in the expansion of an element differ by 2. This simply comes back to the fact that, any given order of an element differs from a higher order one by adding an even number of the virtual currents, as required by the transforms of states to the vacuum [7]. So the expansion for an element in $\boldsymbol{k}_*$ block looks like

$$\langle \boldsymbol{k}'_{*\boldsymbol{q}'}|\underline{\hat{V}}|\boldsymbol{k}_{*\boldsymbol{q}}\rangle_{\boldsymbol{k}_*} = \gamma^h(c_0 + c_2\gamma^2 + c_4\gamma^4 + c_6\gamma^6 + \cdots), \tag{28}$$

in which "h" is the lowest order at which the transforms of both initial and final states to the vacuum are made possible. As the consequence, the expansion is in powers of $1/g^4$, which makes it fairly reliable for even not so large "g." The value of "h" can be determined as well, once $\boldsymbol{k}_*$, $\boldsymbol{q}$, and $\boldsymbol{q}'$ are given. To make things systematically, we use the convention that the representative vector would have the minimum value of

$$|\boldsymbol{k}_*| = \sum_{l=1}^{N_{\mathrm{L}}} |k_{*l}|. \tag{29}$$

The value of "h" is determined once $\boldsymbol{q}$ and $\boldsymbol{q}'$ of (8) and (10) are given, as follows [7]

$$h = |\boldsymbol{k}_*| + |\boldsymbol{q}| + |\boldsymbol{q}'| \tag{30}$$

in which

$$|\boldsymbol{q}| = \sum_{p=1}^{N_{\mathrm{P}}} |q_p|, \qquad |\boldsymbol{q}'| = \sum_{p=1}^{N_{\mathrm{P}}} |q'_p|. \tag{31}$$

III. GAUSS LAW CONSTRAINT IN FOURIER BASIS

It is known that in the procedure of quantization of lattice gauge theories, due to the compact nature of gauge fields, the gauge fixing condition is not needed in the path integral [11,12]. However, it is still necessary to restrict the available states to the gauge-invariant ones, represented by the so-called Wilson loops in the field basis [11,12]. The same is true in the temporal gauge used to derive the transfer-matrix elements in the Fourier basis [7,8]. That is so because, as the result of partial gauge fixing condition $A^0 \equiv 0$, the model still enjoys residual gauge symmetry, acting as time-independent (spatial) gauge transformations [14,15]. In the case of the temporal gauge, it is known that the gauge invariance condition on the states is nothing but the Gauss law constraint [14,15]. In other words, the generator of the spatial gauge transformation, appearing in the Gauss law, should leave the physical states unaffected [14,15]. Accordingly, it is shown that in the temporal gauge the set of physical states consists of the Wilson loops entirely lying in the spatial directions [15]. In the field basis, the wave function corresponding to the spatial Wilson loop is represented by the path-ordered exponential around the spatial closed loop "C" as [11,15]

$$\psi_{\mathrm{C}}[\boldsymbol{\theta}] = \exp\left[\mathrm{i}\sum_{l\in\mathrm{C}} J_l\theta^l\right] \tag{32}$$

in which, depending on the direction of "C" on link l, $J_l = \pm J$ [11]. It is obvious that by construction (32) is gauge invariant. The most general gauge-invariant wave functions are simply constructed by multiplications of those like (32) for a single loop. It is the purpose of this section to map the above physical states in the field basis to the Fourier basis. The transform to the Fourier basis is simply

$$\tilde{\psi}_{\mathrm{C}}[\boldsymbol{k}] = \frac{1}{(2\pi)^{N_{\mathrm{L}}/2}}\int_{-\pi}^{\pi}\prod_l \mathrm{d}\theta_l \exp\left[\mathrm{i}\left(\sum_{l\in\mathrm{C}} J_l\theta^l - \boldsymbol{k}\cdot\boldsymbol{\theta}\right)\right], \tag{33}$$

leading to the following as the product of Kronecker δs of integer values:

$$\tilde{\psi}_{\mathrm{C}}[\boldsymbol{k}] = (2\pi)^{N_{\mathrm{L}}/2}\prod_{l\in\mathrm{C}}\delta(k_l - J_l)\prod_{l'\notin\mathrm{C}}\delta(k_{l'}), \tag{34}$$

by which the gauge invariant state in the Fourier basis has only nonzero currents $|J_l| = J$ along the closed spatial loop "C" of $\psi_{\mathrm{C}}[\boldsymbol{\theta}]$. The identification of the above states is particularly simple by the notions presented in the previous section. For the case of the 1D periodic spatial lattice, the only closed loop is the one around the entire the periodic spatial direction. As in this case, the transfer matrix is diagonal [16,17], and the element for a periodic lattice with N_{L} links finds the following form:

$$\langle k|\hat{V}|k\rangle = \mathcal{A}(e^{-\gamma}\mathrm{I}_k(\gamma))^{N_{\mathrm{L}}}, \quad k = 0, \pm1, \pm2, \ldots, \tag{35}$$

where $\mathcal{A}$ is inserted to fix the normalization [13]. By the elements of diagonal $\hat{V}$, the exact spectrum of 1D model is found [16,17]:

$$E_k = -\frac{1}{a}\ln\langle k|\hat{V}|k\rangle. \tag{36}$$

Above, due to the property of the Bessel functions $\mathrm{I}_0 > \mathrm{I}_{\pm1} > \mathrm{I}_{\pm2}\cdots$, the ground state is given by $k = 0$ [16,17]. In [13], the normalization $\mathcal{A}$ is fixed in a such way that in the weak coupling limit $\gamma \gg 1$, using the asymptotic behavior of Bessel functions:

$$\mathrm{I}_k(\gamma) \simeq \frac{e^{\gamma}}{\sqrt{2\pi\gamma}} e^{-(k^2-1/4)/(2\gamma)}\left[1 + \mathrm{O}\left(\frac{1}{\gamma^2}\right)\right], \quad \gamma \gg k, \tag{37}$$

the continuum energy density (energy per link) expected by the classical model is recovered

$$\frac{E_k}{N_{\mathrm{L}}} \simeq \frac{(k^2 - 1/4)g^2}{2a}, \quad g \ll 1, \qquad k \in \mathbb{Z}. \tag{38}$$

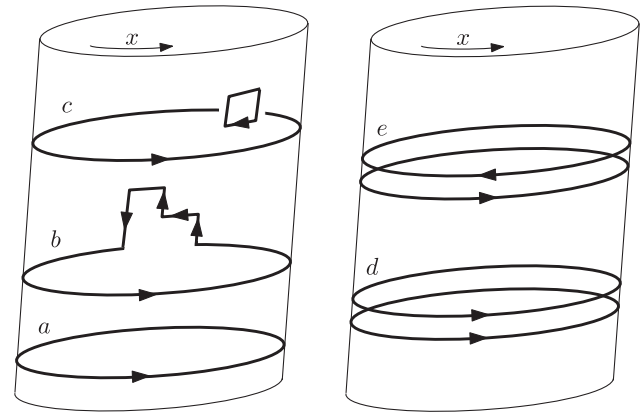

FIG. 6. Left: the periodic loop current a and two of its coblocks b and c. Right: d as a two spaced equal periodic loop currents, and e as a two spaced opposite periodic loop currents. In fact, e belongs to the vacuum block.

For the case of an infinite 1D lattice, one still can define $\tilde{\psi}_{\mathrm{C}}[k]$ along the spatial direction, by which the above finite continuum energy density is valid in the limit $N_{\mathrm{L}} \to \infty$.

For the case of more than one dimension, it is still possible to consider the current-loops around the entire periodic directions, such as in Figs. 6 and 7. As will be seen in the next section, the blocks owners of these periodic large current loops are again responsible for the continuum spectrum expected in the weak coupling limit. However, in the strong coupling limit $\gamma \ll 1$, these periodic loop currents and their blocks contribute only to the extremely excited energies [7]. This can be understood easily by the strong coupling expansion of [7], reviewed in the previous section. Accordingly, the matrix element associated with the mentioned states behaves as $\gamma^{N_{\mathrm{L}}}$ or with higher powers in the limit $\gamma \ll 1$, leading to extremely high energies in the large size limit $N_{\mathrm{L}} \gg 1$ by $E = -N_{\mathrm{L}}\ln\gamma$.

Apart from above-mentioned loops along periodic directions, there are other loops with less number of links in more than one dimension as well. Examples of such closed currents in the 2D spatial lattice are given in Fig. 8. Further examples in a 3D lattice, such as currents at edges are given in Fig. 9, and in general form in Fig. 10. All of these closed currents can be constructed by superposition of equal plaquette currents of the previous section, as shown in each case. As a consequence, all of these gauge invariant finite

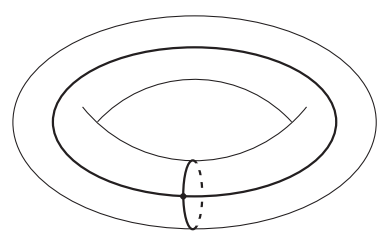

FIG. 7. A gauge invariant Fourier state that consists of two periodic loop-currents along two spatial directions. The two currents are not necessarily equal.

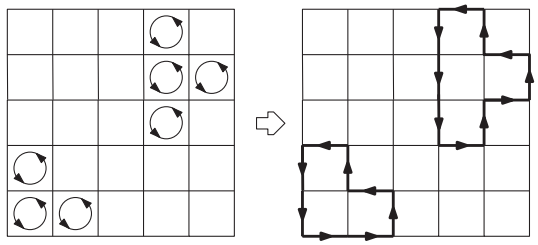

FIG. 8. Examples of 2D gauge invariant closed currents from the vacuum block.

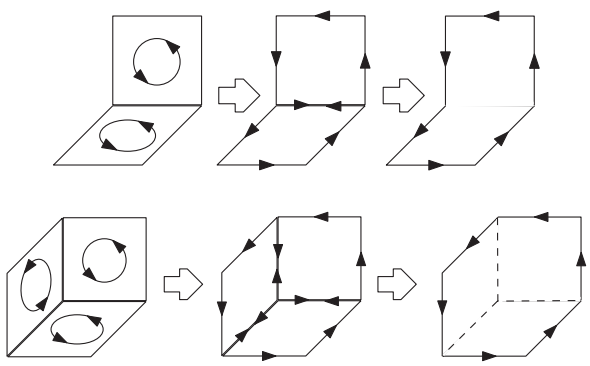

FIG. 9. Examples of 3D closed edge currents from the vacuum block.

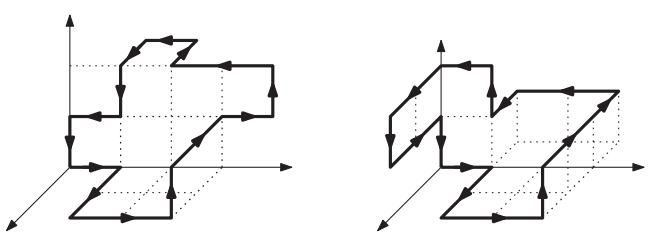

FIG. 10. General 3D closed currents from the vacuum block.

size closed currents belong to the vacuum block. In the previous section, it is seen how the above closed currents are generated by adding the plaquette currents to the vacuum. By the strong coupling expansion of the previous section, a closed current generated by n_c number of the plaquette currents leads to the matrix element $\langle n_c|\underline{\hat{V}}|n_c\rangle \simeq \gamma^{2n_c}$ in the limit $\gamma \ll 1$. This leads to the fact that, in the strong coupling regime, the spectrum of the model comes effectively from the vacuum block; as mentioned before, the other blocks of the periodic loop currents generate only extremely excited energies. As shown in [7], by means of simple perturbative methods, the eigenvalues of the vacuum block can be evaluated in the strong coupling regime [7].

IV. TRANSFER-MATRIX IN WEAK COUPLING LIMIT

The quantum theory of pure U(1) gauge model in the presence of source J_μ may be defined by means of the path integral

$$\mathcal{Z}[J] = \int \mathcal{D}A \exp\left[\mathrm{i}\int \mathrm{d}x\left(-\frac{1}{2}A^\mu(\eta_{\mu\nu}\Box - \partial_\mu\partial_\nu)A^\nu + J_\mu A^\mu\right)\right] \tag{39}$$

leading to

$$\mathcal{Z}[J] \propto |\det(\eta_{\mu\nu}\Box - \partial_\mu\partial_\nu)|^{-1/2}. \tag{40}$$

However, the above expression is infinite due to the zero modes of the operator, corresponding to the pure gauge configurations $A_\mu = \partial_\mu f(x)$:

$$(\eta_{\mu\nu}\Box - \partial_\mu\partial_\nu)\partial^\nu f(x) = \Box\partial_\mu f - \partial_\mu\Box f = 0. \tag{41}$$

The above-mentioned infinity, in other words, is due to the infinite group volume, resulting from integration over $[-\infty, \infty]$ of redundant gauge degrees. Accordingly, the common recipe to avoid the divergent behavior is to fix the gauge. Among many possibilities, one may impose the temporal gauge used in the present work $A^0 = 0$, which is known as an incomplete gauge due to the residual gauge freedom. To make the gauge fixing complete, the so-called Coulomb gauge condition by $\boldsymbol{\nabla}\cdot\boldsymbol{A} = 0$ may be added.

It is commonly expressed that in the lattice formulation of gauge theories, the above mentioned gauge fixing is not necessary. This simply is due to the compact nature of gauge fields $-\pi/g \le aA \le \pi/g$, by which the integration over unfixed gauge degrees would not lead to infinity. In going from the lattice theory to continuum, however, one has to care about the diverging integrals. The main purpose of the present section is to show in detail how the infinities emerge in going to the extreme weak coupling limit $g \to 0$ of the lattice model. In particular, it is seen how the group volume emerges through integration over the zero modes of the operator by the quadratic action in $g \to 0$ limit. The number of mentioned zero modes is equal to the number of "fixing" spots on lattice by the condition $\boldsymbol{\nabla}\cdot\boldsymbol{A} = 0$, and also the number of pure gauge field configurations, both equal to the number of the lattice sites.

In the weak coupling limit $g \ll 1$ the configurations with $\theta \ll 1$ find the dominant contribution. So the cosines in the action can be expanded, leading to the quadratic form similar to the continuum model of gauge theory. Back from the angle variable $\theta = agA$ to the original variables "A," inserted in the following vector with $2N_\mathrm{L}$ components

$$\boldsymbol{\eta} = \begin{pmatrix} \boldsymbol{A} \\ \boldsymbol{A}' \end{pmatrix}, \tag{42}$$

the elements of the transfer matrix are given by means of the following quadratic action

$$\langle\boldsymbol{\theta}'|\hat{V}|\boldsymbol{\theta}\rangle = \mathcal{A}\,\exp\left(-\frac{a^2}{2}\boldsymbol{\eta}^T\boldsymbol{C}\boldsymbol{\eta} + \mathrm{O}(g^2)\right) \tag{43}$$

in which matrix $\boldsymbol{C}$ has $2N_{\mathrm{L}} \times 2N_{\mathrm{L}}$ dimensions, given explicitly by

$$\boldsymbol{C} = \begin{pmatrix} 1 & -1 \\ -1 & 1 \end{pmatrix} \otimes \mathbb{1}_{\mathrm{L}} + \frac{1}{2}\mathbb{1}_2 \otimes \boldsymbol{M}^T\boldsymbol{M}, \tag{44}$$

$$= \left(\begin{array}{c|c} \mathbb{1}_{\mathrm{L}} + \frac{1}{2}\boldsymbol{M}^T\boldsymbol{M} & -\mathbb{1}_{\mathrm{L}} \\ \hline -\mathbb{1}_{\mathrm{L}} & \mathbb{1}_{\mathrm{L}} + \frac{1}{2}\boldsymbol{M}^T\boldsymbol{M} \end{array}\right), \tag{45}$$

with $\mathbb{1}_2$ and $\mathbb{1}_{\mathrm{L}}$ as two- and N_{L}-dimensional identity matrices, respectively. From now on we set $a = 1$, which can be recovered easily by dimensional considerations. To transfer to the Fourier basis, we define the vector

$$\boldsymbol{\kappa} = \begin{pmatrix} \boldsymbol{k} \\ -\boldsymbol{k}' \end{pmatrix} \tag{46}$$

by which, using (6) with original "A" variables, we have

$$\langle \boldsymbol{k}'|\hat{V}|\boldsymbol{k}\rangle \simeq \mathcal{A}\frac{g^{2N_{\mathrm{L}}}}{(2\pi)^{N_{\mathrm{L}}}}\int_{-\pi/g}^{\pi/g} \mathrm{d}\boldsymbol{\eta}\, \exp\left(-\frac{1}{2}\boldsymbol{\eta}^T\boldsymbol{C}\boldsymbol{\eta} + \mathrm{i}g\boldsymbol{\eta}^T\boldsymbol{\kappa}\right). \tag{47}$$

In the limit $g \to 0$ the above integral is practically the Gaussian one. However, at first the zero eigenvalues of matrix $\boldsymbol{C}$ should be treated. The origin of these zero eigenvalues simply goes back to the fact that, in the present temporal gauge $A_0 \equiv 0$, there are still unfixed gauge freedoms. These unfixed degrees contribute infinitely due to the volume of the group in the uncompact limit $g \to 0$. The matrix $\boldsymbol{C}$ is symmetric, so there is a basis in which it is diagonal. In fact, by the eigenvectors of $\boldsymbol{C}$ one can construct the matrix $\boldsymbol{P}$, by which

$$\tilde{\boldsymbol{C}} = \boldsymbol{P}^{-1}\boldsymbol{C}\boldsymbol{P}, \tag{48}$$

$$\tilde{\boldsymbol{\eta}} = \boldsymbol{P}^{-1}\boldsymbol{\eta}, \tag{49}$$

$$\tilde{\boldsymbol{\eta}}^T = \boldsymbol{\eta}^T\boldsymbol{P}, \tag{50}$$

$$\tilde{\boldsymbol{\kappa}} = \boldsymbol{P}^{-1}\boldsymbol{\kappa}, \tag{51}$$

with $\tilde{\boldsymbol{C}}$ being diagonal. By the expectations from the continuum model, we expect that the matrix $\boldsymbol{C}$ has zero eigenvalues. These eigenvalues corresponds to the pure gauge field configurations as (41), by which $\boldsymbol{E} = \boldsymbol{B} = \boldsymbol{0}$. Accordingly, the diagonal matrix may be represented in the following way

$$\tilde{\boldsymbol{C}} = \left(\begin{array}{c|c} \tilde{\boldsymbol{C}}_{\mathrm{u}} & \boldsymbol{0} \\ \hline \boldsymbol{0} & \tilde{\boldsymbol{C}}_{\mathrm{d}} \end{array}\right), \tag{52}$$

where $\tilde{\boldsymbol{C}}_{\mathrm{u}}$ is diagonal and $\tilde{\boldsymbol{C}}_{\mathrm{d}} = \boldsymbol{0}$. The dimension of the subspace by the zero modes determines the size of block $\tilde{\boldsymbol{C}}_{\mathrm{d}} = \boldsymbol{0}$. As zero modes are being represented by the pure gauge configurations as $\boldsymbol{A}(\boldsymbol{x}) = \boldsymbol{\nabla} f(\boldsymbol{x})$, the size is expected to be the number of possible configurations in the coordinate $\boldsymbol{x}$ space, being effectively the number of sites in the lattice version of the model. For the periodic spatial lattices with N_s sites in each direction, by the explicit representation of the matrix $\boldsymbol{M}$, one can check that it is in fact the case, as summarized in Table I. In Appendix A a detailed comparison between the lattice model in the weak coupling limit and the continuum model is presented. In particular, using the explicit representations of matrices $\boldsymbol{C}$ and $\boldsymbol{M}$ for 2D and 3D models, it is shown how the models on the lattice and continuum act similarly in the above-mentioned respects.

TABLE I. For periodic lattices in two and three dimensions the size of block $\tilde{\boldsymbol{C}}_{\mathrm{d}}$ is given by explicit representations of $\boldsymbol{M}$.

	No. of sites	No. of links	dim. of $\tilde{\boldsymbol{C}}_{\mathrm{d}}$
2D lattice	N_s^2	$N_{\mathrm{L}} = 2N_s^2$	$N_{\mathrm{d}} = N_s^2 + 1$
3D lattice	N_s^3	$N_{\mathrm{L}} = 3N_s^3$	$N_{\mathrm{d}} = N_s^3 + 2$

The projection of $\tilde{\boldsymbol{\kappa}}$ on the subspace by $\tilde{\boldsymbol{C}}_{\mathrm{d}}$, denoted by $\tilde{\boldsymbol{\kappa}}_{\mathrm{d}}$, do not appear in the quadratic part $\boldsymbol{\eta}^T\boldsymbol{C}\boldsymbol{\eta}$. Back to the angle variables $\theta = gA$ for these zero modes, upon integration over $\theta \in [-\pi, \pi]$, the Kronecker δs are developed, leading to

$$\langle \boldsymbol{k}'|\hat{V}|\boldsymbol{k}\rangle = \mathcal{A}\frac{g^{2N_{\mathrm{L}}-N_{\mathrm{d}}}}{(2\pi)^{N_{\mathrm{L}}-N_{\mathrm{d}}}}\delta(\tilde{\boldsymbol{\kappa}}_{\mathrm{d}})\int_{-\pi/g}^{\pi/g}\mathrm{d}\tilde{\boldsymbol{\eta}}_{\mathrm{u}} \times \exp\left(-\frac{1}{2}\tilde{\boldsymbol{\eta}}_{\mathrm{u}}^T\tilde{\boldsymbol{C}}_{\mathrm{u}}\tilde{\boldsymbol{\eta}}_{\mathrm{u}} + \mathrm{i}g\tilde{\boldsymbol{\eta}}_{\mathrm{u}}^T\tilde{\boldsymbol{\kappa}}_{\mathrm{u}}\right), \tag{53}$$

in which only integrals on nonzero modes are left. By the explicit representation of $\boldsymbol{M}$, it is an easy task to see that $\delta(\tilde{\boldsymbol{\kappa}}_{\mathrm{d}})$ is automatically satisfied for members of a block of the transfer matrix, constructed by the relations (8) and (10). So the only remaining job is the integration over the nonzero modes, which is well approximated by Gaussian integrals in the limit $g \to 0$, using the following relation [18,19]:

$$\mathrm{erf}(z) = \frac{2}{\sqrt{\pi}}\int_0^z e^{-x^2}\mathrm{d}x, \quad = 1 - \frac{e^{-z^2}}{\sqrt{\pi}}\sum_{n=0}^{\infty}\frac{(-1)^n(2n-1)!!}{2^n z^{2n+1}} \quad z \gg 1. \tag{54}$$

Accordingly, one has the following for $\Lambda \gg 1$ [18]:

$$\int_{-\Lambda}^{\Lambda} e^{-\frac{1}{2}\vec{x}^T\boldsymbol{F}\vec{x} + \mathrm{i}\vec{B}\cdot\vec{x}}\mathrm{d}^n x = \sqrt{\frac{(2\pi)^n}{\det \boldsymbol{F}}}e^{-\frac{1}{2}\vec{B}^T\boldsymbol{F}^{-1}\vec{B}} + \mathrm{O}\left(\frac{e^{-\Lambda^2/2}}{\Lambda}\right). \tag{55}$$

As mentioned earlier, to satisfy $\delta(\tilde{\boldsymbol{\kappa}}_{\rm d})$ two states must belong to the same block of the transfer matrix. For the states (8) and (10) in the block represented by $\boldsymbol{k}_*$, we find the following explicit form

$$\langle \boldsymbol{k}'_{*\boldsymbol{q}'}|\hat{V}|\boldsymbol{k}_{*\boldsymbol{q}}\rangle = \mathcal{A}\frac{g^{2N_{\rm L}-N_{\rm d}}}{(2\pi)^{N_{\rm L}-N_{\rm d}}}\sqrt{\frac{(2\pi)^{2N_{\rm L}-N_{\rm d}}}{\det\tilde{\boldsymbol{C}}_{\rm u}}} \times\left[\exp\left(-\frac{g^2}{2}\tilde{\boldsymbol{\kappa}}_{\rm u}^T\tilde{\boldsymbol{C}}_{\rm u}^{-1}\tilde{\boldsymbol{\kappa}}_{\rm u}\right)+{\rm O}(ge^{-\pi^2/g^2})\right],\ g\ll 1. \tag{56}$$

The resulted expression presents the exact dependence of matrix elements on the lattice size parameters $N_{\rm L}$ and $N_{\rm d}$, related to the number of sites N_s as given in Table I. This is due to the specific parametrization, by which the derivations and different limits are made possible for any lattice size. In the next section an example of large lattice limit for the spectrum is presented.

V. SPECTRUM AT WEAK COUPLING LIMIT

In Sec. III, it is shown how the continuum spectrum of 1D model is recovered in the weak coupling limit. The spectrum by Eq. (38) is essentially g^2k^2, in which "k" represents the quanta of electric field in "g" units along the spatial direction. Recalling that in the present temporal gauge the momentum of the gauge field is related to the electric field by $\boldsymbol{E}=\dot{\boldsymbol{A}}$, and in absence of the magnetic field in the 1D model, the spectrum consists of only the kinetic term. As we will see, the continuum spectrum expected by the classical model, like that of the 1D model in Sec. III, can be recovered for higher dimensions as well. The main difference between 1D model and higher-dimensional ones is that the transfer matrix of the 1D model is diagonal and in the others it is block diagonal [7,8]. The matrix elements by the previous section show clearly that we are faced with almost equal values in each block, and finding the eigenvalues of the transfer matrix seems challenging. As the consequence, it is needed to go back to the field basis and manipulate the matrix elements to make a practically useful form to find the eigenvalues. Back to (43), we see that by

$$\mathbb{P}=\frac{1}{\sqrt{2}}\left(\begin{array}{c|c}\mathbb{1}_{\rm L} & \mathbb{1}_{\rm L}\\ -\mathbb{1}_{\rm L} & \mathbb{1}_{\rm L}\end{array}\right) \tag{57}$$

the matrix $\boldsymbol{C}$ comes to the form

$$\boldsymbol{C}'=\mathbb{P}^{-1}\boldsymbol{C}\mathbb{P}=\left(\begin{array}{c|c}2\mathbb{1}_{\rm L}+\frac{1}{2}\boldsymbol{M}^T\boldsymbol{M} & 0\\ 0 & \frac{1}{2}\boldsymbol{M}^T\boldsymbol{M}\end{array}\right). \tag{58}$$

By the explicit representations given in Appendix A, it can be easily seen that the eigenvalues of $\boldsymbol{M}^T\boldsymbol{M}$ are non-negative. Accordingly, the zero eigenvalues of matrix $\boldsymbol{C}$ can only happen in the lower right block. The number of these eigenvalues is presented in Table I. By the above representation, the matrix element (43) takes the form (setting again $a=1$)

$$\langle \boldsymbol{A}'|\hat{V}|\boldsymbol{A}\rangle = \mathcal{A}\exp\left(-\frac{1}{2}\boldsymbol{A}^-\left(\mathbb{1}_{\rm L}+\frac{1}{4}\boldsymbol{M}^T\boldsymbol{M}\right)\boldsymbol{A}^- -\frac{1}{2}\boldsymbol{A}^+\left(\frac{1}{4}\boldsymbol{M}^T\boldsymbol{M}\right)\boldsymbol{A}^+\right) \tag{59}$$

in which

$$\boldsymbol{A}^\pm=\boldsymbol{A}\pm\boldsymbol{A}'. \tag{60}$$

The above representation finds very simple form by going to the basis in which $\boldsymbol{M}^T\boldsymbol{M}$ is diagonal. As $\boldsymbol{M}^T\boldsymbol{M}$ is symmetric, there are orthonormal eigenvectors such that

$$\boldsymbol{M}^T\boldsymbol{M}|\boldsymbol{\xi}\rangle = 4\xi^2|\boldsymbol{\xi}\rangle \tag{61}$$

for which $\langle\boldsymbol{\xi}|\boldsymbol{\xi}'\rangle=\delta_{\xi\xi'}$. The form of $4\xi^2$ for eigenvalues is chosen for later convenience. In this basis, obviously the zero eigenvalues only find contribution in the $\boldsymbol{A}^-$ part, and the matrix element (59) finds the form

$$\langle \boldsymbol{A}'|\hat{V}|\boldsymbol{A}\rangle = \mathcal{A}\exp\left(-\frac{1}{2}\sum_{\{\xi=0\}}(A_\xi-A'_\xi)^2 -\frac{1}{2}\sum_{\xi\neq 0}((1+\xi^2)(A_\xi-A'_\xi)^2+\xi^2(A_\xi+A'_\xi)^2)\right), \tag{62}$$

in which $\{\xi=0\}$ is used to emphasize that the zero eigenvalue has degeneracy (see Table I). As will be seen, the zero and nonzero modes correspond to the static and standing wave configurations, respectively. The absence of $A^+_{\xi=0}$ in the above expression, upon doing the Fourier transform, would result in the group volume $(2\pi/g)^{N_{\rm d}}$, as seen in the previous section. The first term in the above is simply the free kinetic term for $A^-_{\xi=0}$ modes. Both the group volume and the contribution by the free part to the spectrum can be recovered by the Fourier transform. In the ξ basis, the Fourier term in (47) takes the form

$$\mathrm{i}g\boldsymbol{\eta}^T\boldsymbol{\kappa} = \mathrm{i}g(\boldsymbol{A}\cdot\boldsymbol{k}-\boldsymbol{A}'\cdot\boldsymbol{k}'), \tag{63}$$

$$=\frac{\mathrm{i}}{2}g\left(\sum_{\{\xi=0\}}(A^+_\xi k^-_\xi+A^-_\xi k^+_\xi)+\sum_{\xi\neq 0}(A^+_\xi k^-_\xi+A^-_\xi k^+_\xi)\right), \tag{64}$$

in which $\boldsymbol{k}^\pm=\boldsymbol{k}\pm\boldsymbol{k}'$. As mentioned, the integration on $A^+_{\xi=0}$ would develop the group volume, together with

$\delta(k_\xi^-) = \delta(k_\xi - k'_\xi)$ for $\xi = 0$ s, which corresponds to $\delta(\tilde{\boldsymbol{\kappa}}_\mathrm{d})$ of the previous section. The deltas are satisfied by the general requirement that $\boldsymbol{k}$ and $\boldsymbol{k}'$ belong to the same block, represented by (8) and (10), $\boldsymbol{k} = \boldsymbol{k}_* + \boldsymbol{q}\cdot\boldsymbol{M}$ and $\boldsymbol{k}' = \boldsymbol{k}_* + \boldsymbol{q}'\cdot\boldsymbol{M}$. The energy by the free modes can be calculated upon integration on $A^-_{\xi=0}$ s through the Fourier transform. As the consequence, the contribution of these modes to the energy, using $k_\xi = k'_\xi$ by the delta for the zero modes, is simply found to be

$$E_\mathrm{free} = \sum_{\{\xi=0\}} \frac{1}{2}\left(\frac{gk_\xi^+}{2}\right)^2 = \sum_{\{\xi=0\}} \frac{g^2k_\xi^2}{2}, \tag{65}$$

which is the free kinetic term on a circle of radius $1/g$. The allowed values for $\boldsymbol{k}$ by the Gauss law are discussed in Sec. III. In the 1D case by Eq. (38), the free kinetic part represents the energy of the constant electric flux in the spatial direction. In the higher-dimensional case the allowed electric fluxes may be a nonuniform one. As an example is the straight flux $\boldsymbol{k}_*$ in Fig. 6(a), which represents a nonuniform flux as it is not repeated along the perpendicular direction, say y. Also, due to the term $\boldsymbol{q}\cdot\boldsymbol{M}$ in $\boldsymbol{k} = \boldsymbol{k}_* + \boldsymbol{q}\cdot\boldsymbol{M}$, the original straight flux $\boldsymbol{k}_*$ may transform to a nonstraight one, or may find an accompanied closed flux loop. Examples of both nonstraight flux and a loop added one are presented in Figs. 6(a) and 6(b), respectively. However, due to the projection to the subspace by the zero modes in (65), it is only the uniform part of the mentioned allowed states that contribute to the free part (65). The projection to the zero modes is simply done by the projection operator

$$P_0 = \sum_{\{\xi=0\}} |\xi\rangle\langle\xi|, \tag{66}$$

which satisfies $P_0^2 = P_0$. By the explicit form of the matrix $\boldsymbol{M}$, it is a simple task to check that the result of the projection of the mentioned allowed states to the subspace by zero modes is a uniform electric flux, an example of which is presented in Fig. 11. The state in Fig. 11, by the convection introduced for labeling the links of a 2D lattice, is given by

$$\boldsymbol{k} = (\underbrace{1,1,\ldots,1}_{N_s^2},\underbrace{0,0,\ldots,0}_{N_s^2})^T, \tag{67}$$

in which "T" is inserted to make it a column vector. Physically, the zero modes by the kinetic term $\dot{\boldsymbol{A}}^2$ are representing the pure electric field configurations, the stability of which forces them to be uniform. We later see that, how the continuum limit of the operator $\boldsymbol{M}^T\boldsymbol{M}$ only admits the uniform electric fields for the free kinetic part. The irrelevance of $\boldsymbol{q}\cdot\boldsymbol{M}$ to the zero mode sector can be understood easily by the action of the projection

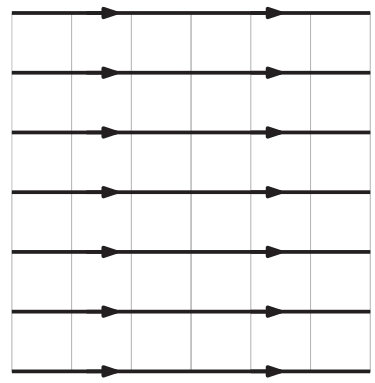

FIG. 11. The thick lines represent $\boldsymbol{k}$ as uniform electric fluxes on links of a 2D lattice.

operator (66). By the fact that the zero modes satisfy $\langle\xi|\boldsymbol{M}^T\boldsymbol{M}|\xi\rangle = |\boldsymbol{M}|\xi\rangle|^2 = 0$, we have

$$P_0(\boldsymbol{q}\cdot\boldsymbol{M})^T = \sum_{\{\xi=0\}} |\xi\rangle\underbrace{\langle\xi|\boldsymbol{M}^T}_{0}\cdot\boldsymbol{q}^T = 0, \tag{68}$$

in which "T" again is inserted to make a column vector.

The nonzero modes in the exponential of (62) represent a harmonic oscillator dynamics, written in the symmetric form in the potential term of the transfer-matrix element

$$\langle x'|\hat{V}|x\rangle = \sqrt{\frac{M}{2\pi}}\exp\left(-\frac{1}{2}M(x-x')^2 - \frac{1}{2}M\omega^2\left(\frac{x+x'}{2}\right)^2\right), \tag{69}$$

with the spectrum $E_r = (r+\frac{1}{2})\omega$ by $r = 0, 1, 2, \ldots$. By the matrix element (62) the frequencies are read as

$$\omega_\xi^2 = \frac{4\xi^2}{1+\xi^2}. \tag{70}$$

The harmonic oscillator nature of this part corresponds to the electromagnetic standing modes inside a resonance cavity. In particular, the electric and magnetic fields of the nonzero modes act as the kinetic and potential terms of an oscillator in the energy density $\frac{1}{2}(\boldsymbol{E}^2 + \boldsymbol{B}^2)$. In the present model the term $\boldsymbol{A}\cdot\boldsymbol{M}^T\boldsymbol{M}\cdot\boldsymbol{A}$ is representing the magnetic part, and the kinetic term $(\boldsymbol{A}-\boldsymbol{A}')^2$ is for the electric part. By the explicit expression for the frequencies, we will see that they in fact correspond to those in a resonance cavity. By (70), it is mentioned that the frequency has an upper limit (ultraviolet cutoff) $\omega_\mathrm{max}^2 = 4$. The existence of the cutoff is simply a consequence of a lower limit of wavelength for a model on the lattice. All together, by adding up the contributions of zero and nonzero modes, after restoring the lattice parameter "a," the spectrum by the model is obtained

$$E_{\rm tot} = \sum_{\{\xi=0\}} \frac{g^2 k_\xi^2}{2a} + \frac{1}{a}\sum_{\xi\neq 0}\left(r_\xi + \frac{1}{2}\right)\omega_\xi. \tag{71}$$

Due to the g^2k^2 part, in the limit $g \ll 1$, the above spectrum is a continuous one. This is equivalent to the case of a particle on a circle with radius R, with momenta and energy as $p = n/R$ and $E = n^2/(2mR^2)$, both being treated as continuous variables in the large R limit. In the present model, the role of the radius is played in the field basis by $1/g$.

It is instructive to have more explicit expression for the frequency of standing modes. By the explicit expression presented in Appendix A, for a 2D periodic lattice with N_s sites in each direction, we have the following for the eigenvalues of $\boldsymbol{M}^T\boldsymbol{M}$ (see Appendix B)

$$4\xi_{m,n}^2 = 4\left(\sin^2\frac{\pi m}{N_s} + \sin^2\frac{\pi n}{N_s}\right), \tag{72}$$

with $m, n = 0, 1, \ldots, N_s - 1$. As mentioned earlier, the present derivations are valid for any lattice size. In particular, the above eigenvalue and related frequency (70) can be applied for arbitrary lattice size. This is an example of the announced feature that the formulation provides the possibility that different limits can be approached. In particular, in the large size limit $N_s \gg 1$, the frequencies can be approximated as

$$\omega_{m,n}^2 \simeq 4\xi_{m,n}^2 = \frac{4a^2\pi^2}{L^2}(m^2+n^2), \quad m, n \ll N_s \tag{73}$$

in which $aN_s = L$ represents the size of the 2D square cavity. The above frequencies are easily recognized as the allowed ones for standing waves in a box with periodic boundary conditions. By the representation given in Appendix A for $\boldsymbol{M}^T\boldsymbol{M}$ in the continuum limit, the standing waves in a square of size L satisfy

$$\begin{pmatrix} -\partial_y^2 & \partial_x\partial_y \\ \partial_x\partial_y & -\partial_x^2 \end{pmatrix}\begin{pmatrix} A(\vec{x},t) \\ A'(\vec{x},t) \end{pmatrix} = \partial_t^2 \begin{pmatrix} A(\vec{x},t) \\ A'(\vec{x},t) \end{pmatrix} \tag{74}$$

in which

$$A(\vec{x},t) = A_0 e^{\frac{2\pi}{L}\mathrm{i}(mx+ny)-\mathrm{i}\omega t}, \tag{75}$$

$$A'(\vec{x},t) = A_0' e^{\frac{2\pi}{L}\mathrm{i}(mx+ny)-\mathrm{i}\omega t}. \tag{76}$$

The condition that for any amplitude A_0 and A_0' there would be a solution as above leads to the frequency (73). The other possibility, relevant to the zero mode sector with $\omega = 0$, is the space independent solution

$$A(\vec{x},t) = A_1 t + A_0, \tag{77}$$

$$A'(\vec{x},t) = A_1' t + A_0', \tag{78}$$

which corresponds to the uniform electric field, as announced earlier. So in the large box limit the spectrum reads

$$E_{\rm tot} = \sum_{\{\xi=0\}} \frac{g^2 k_\xi^2}{2a} + \frac{2\pi}{L}\sum_{m,n}\left(r_{m,n} + \frac{1}{2}\right)\sqrt{m^2+n^2}. \tag{79}$$

The contribution by nonzero modes correspond to the radiation in a cavity. In the large L limit, the discrete nature of the energy levels is relevant only for high frequency modes.

VI. CONCLUSION AND SUMMARY

The weak coupling limit of a lattice gauge model is commonly an obstacle to a full reconciliation between the lattice model and its counterpart on the continuum. In particular, the lattice gauge models are usually transferred to the extreme weak coupling regime in an uncontrolled way, leaving unresolved issues such as an unsought diverging group volume, as well as the unclear fate of main observable quantities in the lattice side, like the Wilson loops.

In the previous sections, it was attempted to improve the procedure of taking the weak coupling limit of a lattice gauge model. Based on the formulation of the transfer matrix in the field Fourier basis, some issues raised by the weak coupling limit of the pure U(1) lattice gauge model in the temporal gauge were addressed. In [7,8], it was shown that the transfer matrix in the Fourier basis is block diagonal. The members of each block can be constructed by a member of the block as the representative [7]. The matrix element between two current states of the same block is directly interpreted as the occurrence of all possible virtual link and loop currents that transform the current states to the vacuum.

One of the basic tools used in the formulation of the transfer matrix in the Fourier basis is the plaquette-link matrix $\boldsymbol{M}$ [7], by which the fields and currents defined on the lattice can be managed in a completely controlled way at any coupling. As a consequence, it is seen that the matrix $\boldsymbol{M}$ provides the possibility to keep and work with the fundamental lattice notions, such as links and sites, even in the extreme weak coupling limit. On the other hand, by Sec. IV and Appendix A, using this matrix enables us to translate the tools on the continuum into the lattice side; examples are the correspondence (A8) between operations $\boldsymbol{M} \leftrightarrow (-\partial_y\partial_x)$, and relations (A11) and (A12). Similar correspondences are presented for 3D lattice as well. These all make it possible to calculate the dimension of the subspace by zero eigenvalues of the operator and to handle the group volume in a safe way, as seen previously. Based on notions and expressions developed in [7], as far as the transfer matrix of the U(1) gauge model in the Fourier basis is concerned, the following clarifications were made:

(1) In the Fourier basis the gauge invariant states identified by the Gauss law constraint consist of Fourier states with equal link current and without boundary. These states, which are known as Wilson loops in the field basis, are either current loops belonging to the vacuum block or states with equal links currents along periodic or infinite spatial directions. In the strong coupling limit, the current loops of the vacuum block have the main contribution to the transfer matrix as well as the spectrum, and link currents along the spatial directions cost an infinite energy. In the weak coupling regime, however, the link currents along spatial directions also find comparable roles.
(2) In the extreme weak coupling limit, the matrix in the quadratic action is identified as the origin of the diverging contributions to the elements of the transfer matrix in the Fourier basis. The states belonging to the subspace corresponding to the zero eigenvalues are clearly interpreted as pure gauge configurations, on which the matrix in the quadratic action vanishes. The dimension of the subspace as well as the diverging volume of the subspace in the weak coupling limit can be handled and extracted in a safe and controlled way.
(3) The spectrum by the lattice model is obtained analytically at the weak coupling limit. The calculation is by means of the very basic notions and tools of the lattice model for any dimension and size of lattice. The obtained spectrum consists of the contribution by the static and standing wave field configurations on the lattice. The spectrum at the weak coupling limit corresponds to the expected one by the continuum model in the large lattice limit.

ACKNOWLEDGMENTS

A. H. F. is grateful to Dr. N. Vadood for providing an earlier explicit representation of matrix $\boldsymbol{M}$ for the 3D lattice. The helpful comments by M. Khorrami on the manuscript are gratefully acknowledged. The authors also would like to thank the anonymous referee for providing detailed and helpful comments leading to correct and improve this work. This work is supported by the Research Council of Alzahra University.

APPENDIX A: MATRICES M AND C FOR 2D AND 3D MODELS

In this Appendix the considerations about the dimension of the subspace by pure gauge configurations, leading to zero eigenvalues of the matrix $\boldsymbol{C}$, is presented. Also, the related notions and elements in both lattice and the continuum models are derived and compared. The following is done for 2D model first, and the very same construction for 3D case is presented shortly. In the temporal gauge $A_0 \equiv 0$, in which

$$\boldsymbol{E} = \dot{\boldsymbol{A}}, \qquad \boldsymbol{B} = \boldsymbol{\nabla} \times \boldsymbol{A} \tag{A1}$$

the Hamiltonian density

$$\mathcal{H} = \frac{1}{2}(\dot{\boldsymbol{A}}^2 + (\boldsymbol{\nabla} \times \boldsymbol{A})^2) \tag{A2}$$

in 2D takes the form

$$\mathcal{H} = \frac{1}{2}(\dot{A}_x^2 + \dot{A}_y^2 + (\partial_x A_y - \partial_y A_x)^2). \tag{A3}$$

By the two-adjacent times interpretation of (5) for the definition of the transfer matrix, the Hamiltonian symmetrized between the variables A and A' at two times, after integration by parts, is

$$\mathcal{H} = \frac{1}{2}\Bigg((A'_x - A_x)^2 + (A'_y - A_y)^2 + \frac{1}{2}[(A_x\partial_y - A_y\partial_x)(\partial_x A_y - \partial_y A_x) + A \to A']\Bigg). \tag{A4}$$

By the definition for the vector $\boldsymbol{\eta}$ as (42), the Hamiltonian density recasts to

$$\mathcal{H} = \frac{1}{2}\boldsymbol{\eta}^T \boldsymbol{C}_{2\mathrm{D}} \boldsymbol{\eta}, \tag{A5}$$

in which

$$\boldsymbol{C}_{2\mathrm{D}} = \begin{pmatrix} 1 & -1 \\ -1 & 1 \end{pmatrix} \otimes \mathbb{1}_{\vec{x}} + \frac{1}{2}\mathbb{1}_2 \otimes \begin{pmatrix} -\partial_y^2 & \partial_x\partial_y \\ \partial_x\partial_y & -\partial_x^2 \end{pmatrix}. \tag{A6}$$

Comparing the above operator with (45) of the lattice formulation, we see that the combination $\boldsymbol{M}^T\boldsymbol{M}$ is in fact acting as the derivative ∂_i in the last 2×2 matrix:

$$\boldsymbol{M}^T\boldsymbol{M} \leftrightarrow \begin{pmatrix} -\partial_y^2 & \partial_x\partial_y \\ \partial_x\partial_y & -\partial_x^2 \end{pmatrix} = \begin{pmatrix} \partial_y \\ -\partial_x \end{pmatrix} \begin{pmatrix} -\partial_y & \partial_x \end{pmatrix}, \tag{A7}$$

which, recalling that ∂_i is an antisymmetric operator ($\partial_i^T = -\partial_i$), leads to the following correspondence

$$\boldsymbol{M} \leftrightarrow \begin{pmatrix} -\partial_y & \partial_x \end{pmatrix}. \tag{A8}$$

The matrix $\boldsymbol{M}$ can be defined by using the $N_s \times N_s$ translation matrix $\boldsymbol{T}$, defined by its elements [8]

$$T_{ab} = \delta_{ab} - \delta_{a+1,b} - \delta_{a,N_s}\delta_{b1}, \quad a, b = 1, \ldots, N_s. \tag{A9}$$

Then, the general form of the matrix $\boldsymbol{M}$ for the 2D lattice is given in [7,8]

$$\boldsymbol{M} = \left(-\boldsymbol{M}_y \;\middle|\; \boldsymbol{M}_x\right), \tag{A10}$$

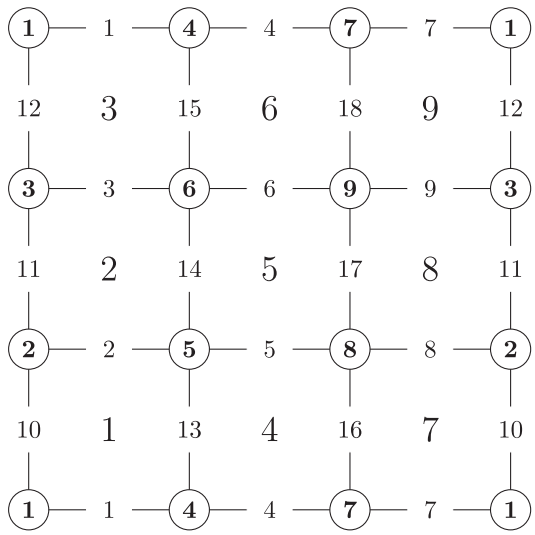

FIG. 12. The numbering of links and plaquettes for the 3×3 2D periodic lattice used in (19) as the representation of matrix $\boldsymbol{M}$ [8].

by which, using (A8), we have

$$\boldsymbol{M}_x = -\boldsymbol{T} \otimes \mathbb{1}_{N_s} \longleftrightarrow \partial_x, \tag{A11}$$

$$\boldsymbol{M}_y = -\mathbb{1}_{N_s} \otimes \boldsymbol{T} \longleftrightarrow \partial_y. \tag{A12}$$

By construction, the matrix $\boldsymbol{M}$ is $N_s^2 \times 2N_s^2$ dimensional, as it should be for the 2D lattice. The similarity between the lattice formulation in the weak coupling limit and the continuum model in fact goes further, as both operators vanish acting on a gradient. For the above operator the gradient of function is

$$\boldsymbol{\nabla} f = \begin{pmatrix} \partial_x f \\ \partial_y f \end{pmatrix} \tag{A13}$$

and obviously satisfies

$$\begin{pmatrix} -\partial_y & \partial_x \end{pmatrix} \begin{pmatrix} \partial_x f \\ \partial_y f \end{pmatrix} = 0. \tag{A14}$$

In the lattice side, the gradient of a function is simply given by (A11) and (A12). Let us use the notation that the function "f" at site "i" is denoted as f_i. Then the column vector is defined as

$$\vec{f} = (f_1, f_2, \ldots, f_{N_s^2})^T, \tag{A15}$$

in which "T" is inserted to make it a column vector. Using (A11) and (A12), the gradient on lattice is then defined as

$$\boldsymbol{\Delta} f = \begin{pmatrix} \Delta_x f \\ \Delta_y f \end{pmatrix} = \begin{pmatrix} \boldsymbol{M}_x \vec{f} \\ \boldsymbol{M}_y \vec{f} \end{pmatrix}, \tag{A16}$$

which, using $\boldsymbol{M}_x \boldsymbol{M}_y = \boldsymbol{M}_y \boldsymbol{M}_x$ by the given representations, satisfies

$$\boldsymbol{M} \cdot \begin{pmatrix} \Delta_x f \\ \Delta_y f \end{pmatrix} = \begin{pmatrix} -\boldsymbol{M}_y & \boldsymbol{M}_x \end{pmatrix} \begin{pmatrix} \boldsymbol{M}_x \vec{f} \\ \boldsymbol{M}_y \vec{f} \end{pmatrix} = 0. \tag{A17}$$

It is useful to have an explicit representation for the plaquette-link matrix $\boldsymbol{M}$. For the site, plaquette and link numberings of the 3×3 periodic lattice given in Fig. 12, using the definition (3), one finds the following form for the (9×18)-dimensional matrix $\boldsymbol{M}$ [8]

$$\boldsymbol{M} = \left(\underbrace{\begin{matrix} + & - & 0 & 0 & 0 & 0 & 0 & 0 & 0 \\ 0 & + & - & 0 & 0 & 0 & 0 & 0 & 0 \\ - & 0 & + & 0 & 0 & 0 & 0 & 0 & 0 \\ 0 & 0 & 0 & + & - & 0 & 0 & 0 & 0 \\ 0 & 0 & 0 & 0 & + & - & 0 & 0 & 0 \\ 0 & 0 & 0 & - & 0 & + & 0 & 0 & 0 \\ 0 & 0 & 0 & 0 & 0 & 0 & + & - & 0 \\ 0 & 0 & 0 & 0 & 0 & 0 & 0 & + & - \\ 0 & 0 & 0 & 0 & 0 & 0 & - & 0 & + \end{matrix}}_{-\boldsymbol{M}_y} \underbrace{\begin{matrix} - & 0 & 0 & + & 0 & 0 & 0 & 0 & 0 \\ 0 & - & 0 & 0 & + & 0 & 0 & 0 & 0 \\ 0 & 0 & - & 0 & 0 & + & 0 & 0 & 0 \\ 0 & 0 & 0 & - & 0 & 0 & + & 0 & 0 \\ 0 & 0 & 0 & 0 & - & 0 & 0 & + & 0 \\ 0 & 0 & 0 & 0 & 0 & - & 0 & 0 & + \\ + & 0 & 0 & 0 & 0 & 0 & - & 0 & 0 \\ 0 & + & 0 & 0 & 0 & 0 & 0 & - & 0 \\ 0 & 0 & + & 0 & 0 & 0 & 0 & 0 & - \end{matrix}}_{\boldsymbol{M}_x} \right). \tag{A18}$$

By the representation, the gradient based on the given ordering of sites and links for the 3×3 periodic lattice, denoting $f_{ij} = f_j - f_i$, is the following:

$$\Delta f = \begin{pmatrix} \boldsymbol{M}_x \vec{f} \\ \boldsymbol{M}_y \vec{f} \end{pmatrix} = (f_{41}, f_{52}, f_{63}, f_{74}, f_{85}, f_{96}, f_{17}, f_{28}, f_{39}, f_{21}, f_{32}, f_{13}, f_{54}, f_{65}, f_{46}, f_{87}, f_{98}, f_{79})^T. \tag{A19}$$

We notice that, for example, f_{63} is sitting in place of the variable on link "3," consistent by the numbering given in Fig. 12.

In the language of gauge theories, the expressions (A13) and (A16) are referred as pure gauge configurations. In fact, in the present temporal gauge $A_0 \equiv 0$, starting with zero field configurations in two adjacent times given by $\boldsymbol{A} = \boldsymbol{A}' = 0$, the remaining spatial gauge transformations leads to $\boldsymbol{A} = \boldsymbol{A}' = \boldsymbol{\nabla} f$ in the continuum theory, and $\boldsymbol{A} = \boldsymbol{A}' = \boldsymbol{\Delta} f$ in the lattice one. As expected, by the pure gauge configurations (A13) and (A16), the Hamiltonian vanishes, leading to vanishing of the strength fields: $\boldsymbol{E} = \boldsymbol{B} = \boldsymbol{0}$.

It is instructive to see that the construction for the 2D model can be directly generalized to the 3D one. By the two-adjacent times interpretation in the definition of the transfer matrix, the Hamiltonian symmetrized between the variables A and A' at two times, after integration by parts, takes the following form in 3D

$$\begin{aligned}\mathcal{H} = \frac{1}{2}\Big(&(A'_x - A_x)^2 + (A'_y - A_y)^2 + (A'_z - A_z)^2 \\ &+ \frac{1}{2}[(A_x\partial_y - A_y\partial_x)(\partial_x A_y - \partial_y A_x) + A \to A' \\ &+ (A_y\partial_z - A_z\partial_y)(\partial_y A_z - \partial_z A_y) + A \to A' \\ &+ (A_z\partial_x - A_x\partial_z)(\partial_z A_x - \partial_x A_z) + A \to A']\Big) \end{aligned} \tag{A20}$$

written in matrix form

$$\mathcal{H} = \frac{1}{2}\boldsymbol{\eta}^T \boldsymbol{C}_{3\mathrm{D}} \boldsymbol{\eta}, \tag{A21}$$

in which

$$\begin{aligned}\boldsymbol{C}_{3\mathrm{D}} = &\begin{pmatrix} 1 & -1 \\ -1 & 1 \end{pmatrix} \otimes \mathbb{1}_{\vec{x}} \\ &+ \frac{1}{2}\mathbb{1}_2 \otimes \begin{pmatrix} -\partial_y^2 - \partial_z^2 & \partial_x\partial_y & \partial_x\partial_z \\ \partial_x\partial_y & -\partial_x^2 - \partial_z^2 & \partial_z\partial_y \\ \partial_x\partial_z & \partial_z\partial_y & -\partial_x^2 - \partial_y^2 \end{pmatrix}. \end{aligned} \tag{A22}$$

Comparing with (44),

$$\boldsymbol{M}^T\boldsymbol{M} \leftrightarrow \begin{pmatrix} -\partial_y^2 - \partial_z^2 & \partial_x\partial_y & \partial_x\partial_z \\ \partial_x\partial_y & -\partial_x^2 - \partial_z^2 & \partial_z\partial_y \\ \partial_x\partial_z & \partial_z\partial_y & -\partial_x^2 - \partial_y^2 \end{pmatrix} \tag{A23}$$

$$= \begin{pmatrix} \partial_y & \partial_z & 0 \\ -\partial_x & 0 & \partial_z \\ 0 & -\partial_x & -\partial_y \end{pmatrix} \begin{pmatrix} -\partial_y & \partial_x & 0 \\ -\partial_z & 0 & \partial_x \\ 0 & -\partial_z & \partial_y \end{pmatrix}. \tag{A24}$$

For a periodic 3D lattice with N_s sites in each direction we have for the number of links and plaquettes

$$N_{\mathrm{L}} = N_{\mathrm{P}} = 3N_s^3, \tag{A25}$$

suggesting

$$\boldsymbol{M} = \left(\begin{array}{c|c|c} -\boldsymbol{M}_y & \boldsymbol{M}_x & 0 \\ \hline -\boldsymbol{M}_z & 0 & \boldsymbol{M}_x \\ \hline 0 & -\boldsymbol{M}_z & \boldsymbol{M}_y \end{array}\right) \leftrightarrow \begin{pmatrix} -\partial_y & \partial_x & 0 \\ -\partial_z & 0 & \partial_x \\ 0 & -\partial_z & \partial_y \end{pmatrix} \tag{A26}$$

with

$$\boldsymbol{M}_x = -\boldsymbol{T} \otimes \mathbb{1}_{N_s} \otimes \mathbb{1}_{N_s} \leftrightarrow \partial_x, \tag{A27}$$

$$\boldsymbol{M}_y = -\mathbb{1}_{N_s} \otimes \boldsymbol{T} \otimes \mathbb{1}_{N_s} \leftrightarrow \partial_y, \tag{A28}$$

$$\boldsymbol{M}_z = -\mathbb{1}_{N_s} \otimes \mathbb{1}_{N_s} \otimes \boldsymbol{T} \leftrightarrow \partial_z, \tag{A29}$$

by which as it is required that $\boldsymbol{M}_i\boldsymbol{M}_j = \boldsymbol{M}_j\boldsymbol{M}_i$ for $i, j = x, y, z$.

APPENDIX B: EIGENVALUES OF $\boldsymbol{M}^T\boldsymbol{M}$

The eigenvalues of $\boldsymbol{M}^T\boldsymbol{M}$ for periodic 2D lattice are calculated in this part. The 3D case can be calculated straightforwardly. By the given representation, $\boldsymbol{M}^T\boldsymbol{M}$ for 2D lattice comes to the form

$$\boldsymbol{M}^T\boldsymbol{M} = \left(\begin{array}{c|c} \mathbb{1} \otimes \boldsymbol{T}^\dagger\boldsymbol{T} & -\boldsymbol{T} \otimes \boldsymbol{T}^\dagger \\ \hline -\boldsymbol{T}^\dagger \otimes \boldsymbol{T} & \boldsymbol{T}^\dagger\boldsymbol{T} \otimes \mathbb{1} \end{array}\right), \tag{B1}$$

in which both 1 and $\boldsymbol{T}$ are $N_s \times N_s$ dimensional (as in Appendix A). So $\boldsymbol{M}^T\boldsymbol{M}$ is $2N_s^2 \times 2N_s^2$, as it should. For a block matrix

$$M = \left(\begin{array}{c|c} A & B \\ \hline C & D \end{array}\right), \tag{B2}$$

if C and D commute, then $\det M = \det(AD - BC)$. The calculation is done on the basis that $\boldsymbol{T}$ is diagonal, in which all blocks commute. The secular equation $\det(\boldsymbol{M}^T\boldsymbol{M} - \lambda) = 0$ then finds the form

$$\det(\lambda(\lambda\mathbb{1} \otimes \mathbb{1} - \mathbb{1} \otimes \boldsymbol{T}^\dagger\boldsymbol{T} - \boldsymbol{T}^\dagger\boldsymbol{T} \otimes \mathbb{1})) = 0. \tag{B3}$$

The outer λ leads to N_s^2 number of zeros as eigenvalues. Other eigenvalues, denoting eigenvalues of $\boldsymbol{T}^\dagger\boldsymbol{T}$ as β_m, are simply

$$\lambda_{m,n} = \beta_m + \beta_n, \quad m, n = 0, 1, \ldots, N_s - 1. \tag{B4}$$

The only remaining part is to find the eigenvalues of $\boldsymbol{T}^\dagger\boldsymbol{T}$. By the explicit representation given in Appendix A, the secular equation for $\boldsymbol{T}$ is

$$(1-\alpha)^{N_s} = 1, \tag{B5}$$

with the following as a solution:

$$\alpha_m = 1 - \exp\frac{2\pi \mathrm{i}\, m}{N_s}. \tag{B6}$$

So the eigenvalues of $\boldsymbol{T}^\dagger \boldsymbol{T}$ are

$$\beta_m = \alpha_m \alpha_m^* = 4\sin^2\frac{\pi m}{N_s} \tag{B7}$$

resulting in

$$\lambda_{m,n} = 4\left(\sin^2\frac{\pi m}{N_s} + \sin^2\frac{\pi n}{N_s}\right), \qquad m, n = 0, 1, \ldots, N_s - 1. \tag{B8}$$

[1] R. Savit, Topological Excitations in U(1)-Invariant Theories, Phys. Rev. Lett. **39**, 55 (1977).

[2] T. Banks, R. Myerson, and J. B. Kogut, Phase transitions in abelian lattice gauge theories, Nucl. Phys. **B129**, 493 (1977).

[3] C. Gattringer, New developments for dual methods in lattice field theory at non-zero density, Proc. Sci., LATTICE2013 (**2014**) 002 [arXiv:1401.7788].

[4] S. E. Koonin, E. A. Umland, and M. R. Zirnbauer, U(1) lattice gauge theory in the electric-field representation, Phys. Rev. D **33**, 1795 (1986).

[5] T. Byrnes and Y. Yamamoto, Simulating lattice gauge theories on a quantum computer, Phys. Rev. A **73**, 022328 (2006).

[6] C. Best and A. Schafer, U(1) flux tube profiles from hamiltonian lattice gauge theory using a random walk ground-state projector, Nucl. Phys. B, Proc. Suppl. **42**, 216 (1995).

[7] A. Kianfar and A. H. Fatollahi, Diagrammatic strong coupling expansion of a U(1) lattice model in the fourier basis, Phys. Rev. D **104**, 094506 (2021).

[8] N. Vadood and A. H. Fatollahi, On U(1) gauge theory transfer-matrix in fourier basis, Commun. Theor. Phys. **71**, 921 (2019).

[9] M. Luscher, Construction of a selfadjoint, strictly positive transfer matrix for euclidean lattice gauge theories, Commun. Math. Phys. **54**, 283 (1977).

[10] K. Osterwalder and E. Seiler, Gauge field theories on a lattice, Ann. Phys. (N.Y.) **110**, 440 (1978).

[11] K. G. Wilson, Confinement of quarks, Phys. Rev. D **10**, 2445 (1974).

[12] J. B. Kogut, An introduction to lattice gauge theory and spin systems, Rev. Mod. Phys. **51**, 659 (1979).

[13] N. Vadood and A. H. Fatollahi, Lost in normalization, Europhys. Lett. **131**, 41003 (2020).

[14] M. Cruetz, Gauge fixing, the transfer matrix, and confinement on a lattice, Phys. Rev. D **15**, 1128 (1977).

[15] J. Smit, *Introduction to Quantum Fields on a Lattice* (Cambridge University Press, Cambridge, England, 2002), Chap. 4.

[16] R. Balian, J. M. Drouffe, and C. Itzykson, Gauge fields on a lattice. I. General outlook, Phys. Rev. D **10**, 3376 (1974).

[17] A. Wipf, *Statitical Approach to Quantum Field Theory* (Springer Berlin, Heidelberg, 2013), Chap. 14, 10.1007/978-3-642-33105-3.

[18] M. Abramowitz and I. A. Stegun, *Handbook of Mathematical Functions with Formulas, Graphs, and Mathematical Tables* (Dover, New York, 1972), pp. 297–309.

[19] E. W. Weisstein, Erf. from MathWorld—A Wolfram Web Resource, https://mathworld.wolfram.com/Erf.html.